Supporting Information

Rational design of ion transport paths at the interface of metal-organic framework modified solid electrolyte

Yangyang Xia, [†] Nuo Xu, [†] Lulu Du, [†] Yu Cheng, [†] Shulai Lei, [‡] Shujuan Li, [‡] Xiaobin Liao, [†] Wenchao Shi, [†] Lin Xu*, [†, §] and Liqiang Mai*, [†, §]

[†] State Key Laboratory of Advanced Technology for Materials Synthesis and Processing, International School of Materials Science and Engineering, Wuhan University of Technology, Wuhan 430070, China.

[‡] Hubei Key Laboratory of Low Dimensional Optoelectronic Materials and Devices, Hubei University of Arts and Science, Xiangyang 441053, China.

[§] Foshan Xianhu Laboratory of the Advanced Energy Science and Technology Guangdong Laboratory, Xianhu hydrogen Valley, Foshan 528200, China.

Corresponding Author: * mlq518@whut.edu.cn, * linxu@whut.edu.cn

Experiment details

In view of the pore volume of ZIF-8, the mass ratio of ZIF-8: $(EMIM_{0.83}Li_{0.17})TFSI = 1 : 1$ was selected in the electrochemical characterizations. If the $[ZIF-8:(EMIM_{0.83}Li_{0.17})TFSI]$ mass ratio is slightly greater than 1, the pore volume of ZIF-8 framework cannot be filled because the total pore volume of ZIF-8 is greater than the total volume of $(EMIM_{0.83}Li_{0.17})TFSI$. As for ionic conductivity, lesser $(EMIM_{0.83}Li_{0.17})TFSI$ is insufficient for ionic transport in micropores of ZIF-8.[1] If the $[ZIF-8:(EMIM_{0.83}Li_{0.17})TFSI]$ mass ratio is slightly less than 1, the sample showed a wet-gel state, indicating an excess amount of mixed ionic liquid which could not be absorbed by the ZIF-8 host. The ZIL was completely solidified and remained as "free-flowing" dry powder at the $[ZIF-8: (EMIM_{0.83}Li_{0.17})TFSI]$ mass ratio of 1:1, which could eliminate the risk of liquid leakage.[2] So the proper mass ratio of ZIF-8: $(EMIM_{0.83}Li_{0.17})TFSI = 1 : 1$ was chosen according to the pore volume of ZIF-8.

Characterization of the solid electrolyte

The thickness of the CSE and C-CSE was recorded by a micrometer caliper (Shanghai measuring tool factory, China). The morphology of ZIF-8, CSE and C-CSE was represented by a field-emission scanning electron microscopy (JEOL-7100F) after gold spraying. Energy Dispersive Spectrometer were executed by an Oxford IE250 system. Transmission electron microscope image was characterized using JEM-1400plus. X-ray diffraction (XRD) patterns were recorded using a D8 discover X-ray diffractometer with Cu Kα radiation. The surface area and pore-size distribution were calculated from N_2 adsorption isotherms measured by using a Tristar-3020 instrument. The Fourier Transform Infrared (FT-IR, NICOLET-6700) spectroscopy (400–4000 cm^{-1}) was carried out at 25 °C.

Electrochemical measurements

Electrochemical impedance spectroscopy (EIS) was tested by assembling a blocking stainless steel|SSE|stainless steel cell from 0.1 Hz to 1 MHz with an amplitude of 10 mV via Autolab PGSTAT302N. The electrochemical stability window was tested by linear sweep voltammetry on a lithium|SSE|stainless steel cell from open-circuit voltage to 6.5 V at a scan rate of 5 mV s^{-1}. The lithium compatibility of lithium|SSE|lithium and SSB were conducted using a multichannel battery testing system (LAND CT2001A). The cathode material is commercial cathode material and the mass loading of $LiFePO_4$ is about 8 mg. CR2016 coin cells were assembled with cathode electrode, C-CSE and commercial lithium metal anodes via ordinal stacking.

The measurement of ionic conductivity: The bulk resistance (R_b) of solid-state electrolytes (SSBs) was obtained from the EIS. The ionic conductivity was calculated from Equation (S1):

$$\sigma = \frac{L}{R_b S} \tag{1}$$

where R_b is the bulk resistance of SSE, L is the thickness of the SSE and S is the area of the SSEs.

The measurement of the lithium-ion transference number (t_{Li}^+) : t_{Li}^+ has been measured using the Evans method. Direct current signal is applied to a symmetric lithium|C-CSE|lithium battery. The current through lithium|C-CSE|lithium and the impedance of lithium|C-CSE|lithium before and after the polarization are measured via Autolab. The t_{Li}^+ can be calculated as in Equation (S2):

$$t_{Li^+} = \frac{i_s \times (\Delta V - i_0 R_0)}{i_0 \times (\Delta V - i_s R_s)} \tag{2}$$

where ΔV is the applied signal amplitude of potential, R_0 is the measured resistance values of lithium|C-CSE|lithium before polarization and R_S is the measured resistance values of lithium|C-CSE|lithium at steady state condition after polarization. i_0 is the incipient current in the pristine state and and i_S is the current values measured immediately after polarization and at steady state condition. The calculated t_{Li^+} of the C-CSE$_3$ sample is 0.67 ± 0.08 (Fig. S9b).

The computational formula of the activation energies (Ea): The Ea of solid electrolytes in Figure 3b and Figure S7 was calculated by Arrhenius relation from Equation (S3)[3]:

$$\sigma = A\exp(-\frac{Ea}{kT}) \tag{3}$$

where σ is ionic conductivity of solid electrolyte, A is pre-exponential factor, Ea is activation energy, k is Boltzmann constant, and T is temperature of testing process.

Computational details

First-principles method implemented in the Vienna *ab initio* Simulation Package (VASP) were used to study the geometric and transition states of solid electrolytes based on ZIF. [4,5] The electron-ion interaction was presented by the PAW method and exchange correlation interactions were described by the Perdew-Burke-Ernzerhof generalized gradient approximation. Due to large supercell of ZIF, single K-point was used. The plane wave kinetic energy cutoff was set to be 400 eV and atomic positions and lattice parameters were fully relaxed at the GGA level until the atomic forces were smaller than 0.02 eV/Å.
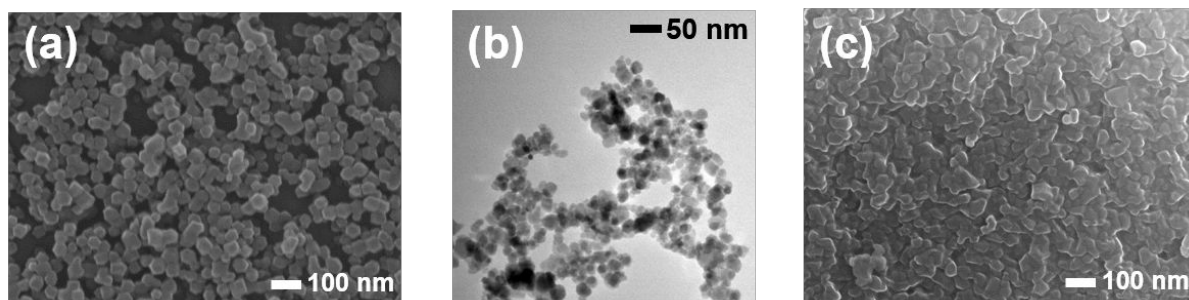
Figure S1. (a) SEM image of ZIF-8. (b) TEM image of ZIF-8. (c) SEM image of porous ZIF-8 loaded with ionic liquid (ZIL).
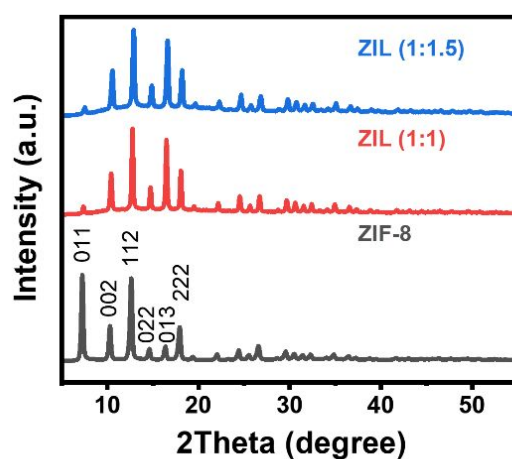
Figure S2. XRD patterns of ZIF-8 and ZIL in a different mass ratio [ZIF-8: $(EMIM_{0.83}Li_{0.17})TFSI = 1:1$ and ZIF-8: $(EMIM_{0.83}Li_{0.17})TFSI = 1:1.5$].
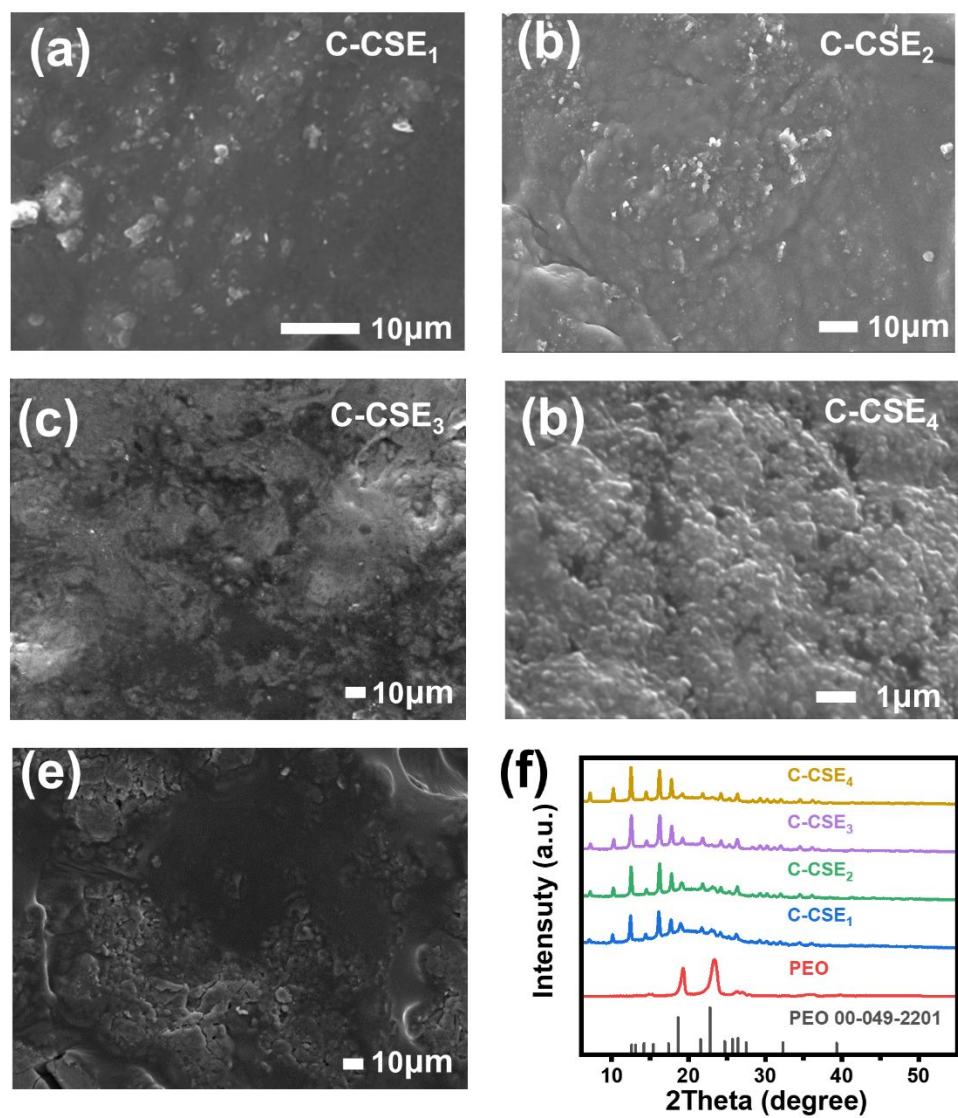
Figure S3. (a) SEM image of C-CSE$_1$. (b) SEM image of C-CSE$_2$. (c) SEM image of C-CSE$_3$. (d) SEM image of C-CSE$_4$. (e) SEM image of CSE. (f) XRD patterns of PEO, C-CSE$_1$, C-CSE$_2$, C-CSE$_3$ and C-CSE$_4$.
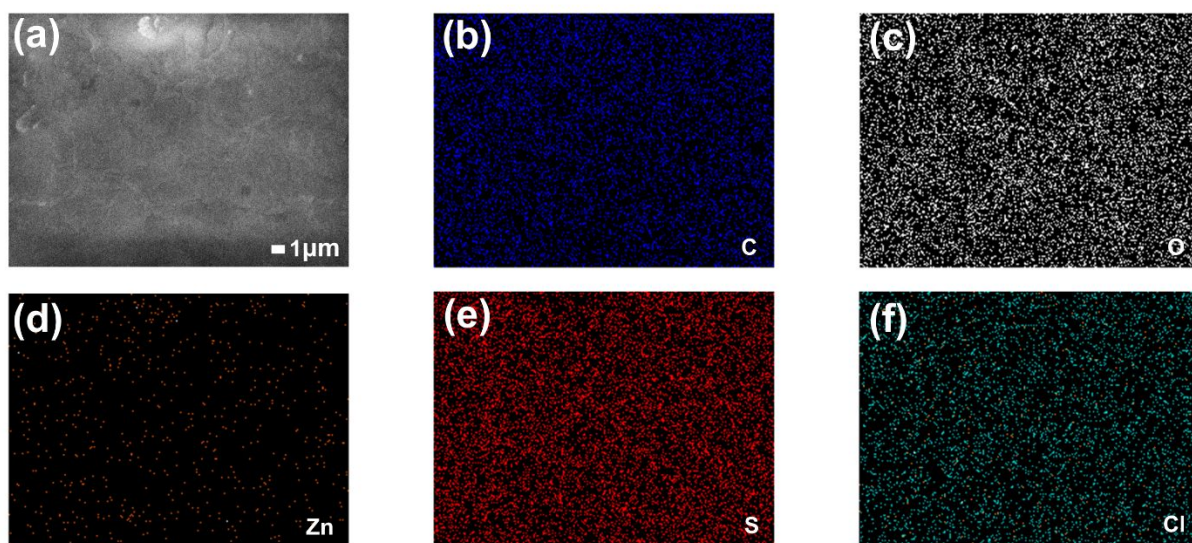
Figure S4. Energy Dispersive Spectrometer of C-CSE$_3$.
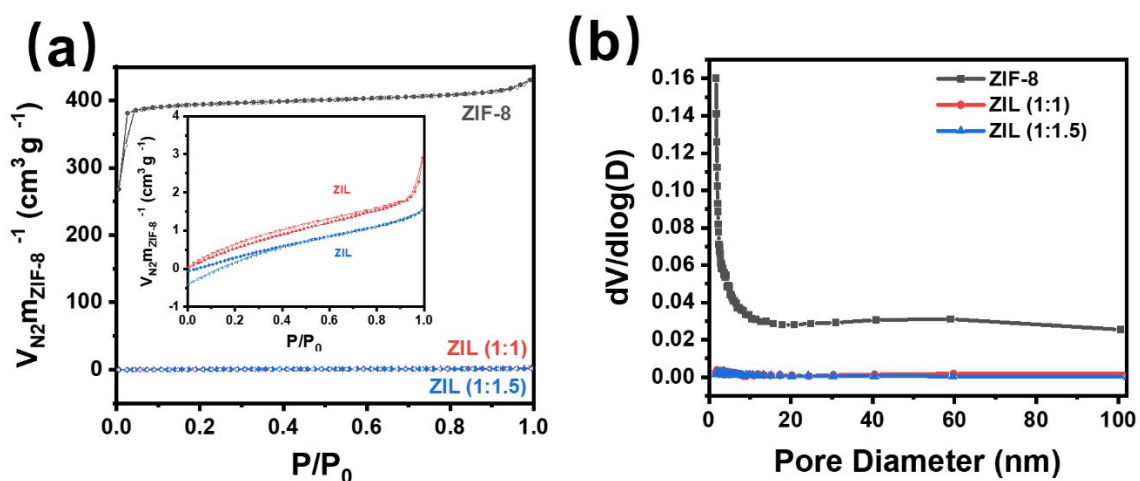
Figure S5. BET of ZIF-8 and ZIL in a different mass ratio [ZIF-8: (EMIM$_{0.83}$Li$_{0.17}$)TFSI = 1:1 and ZIF-8: (EMIM$_{0.83}$Li$_{0.17}$)TFSI = 1:1.5]. (a) Nitrogen gas adsorption isotherms. (b) Pore diameter distribution.
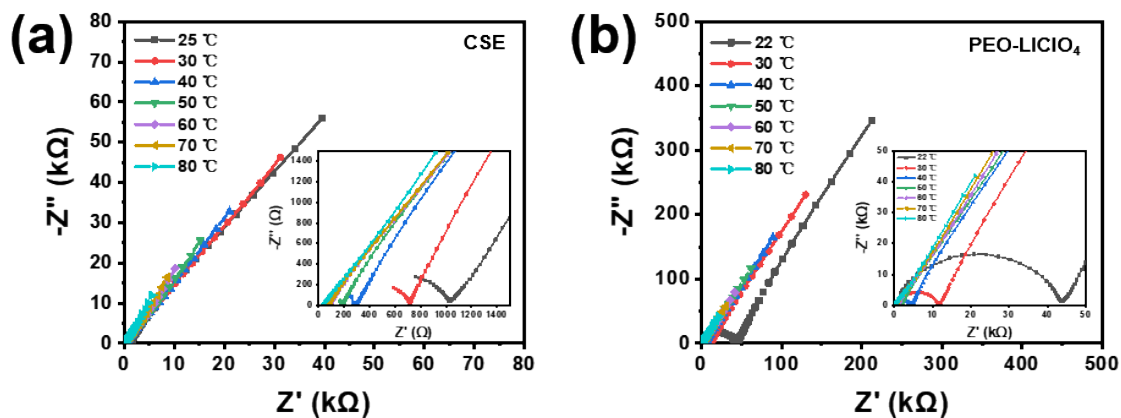
Figure S6. (a) EIS of CSE within frequency of 0.1 Hz–1 MHz at temperatures from 20 °C to 80 °C, inset: magnified high frequency region. (b) EIS of PEO-LiClO$_4$ within frequency of 0.1 Hz–1 MHz at temperatures from 20 °C to 80 °C, inset: magnified high frequency region.
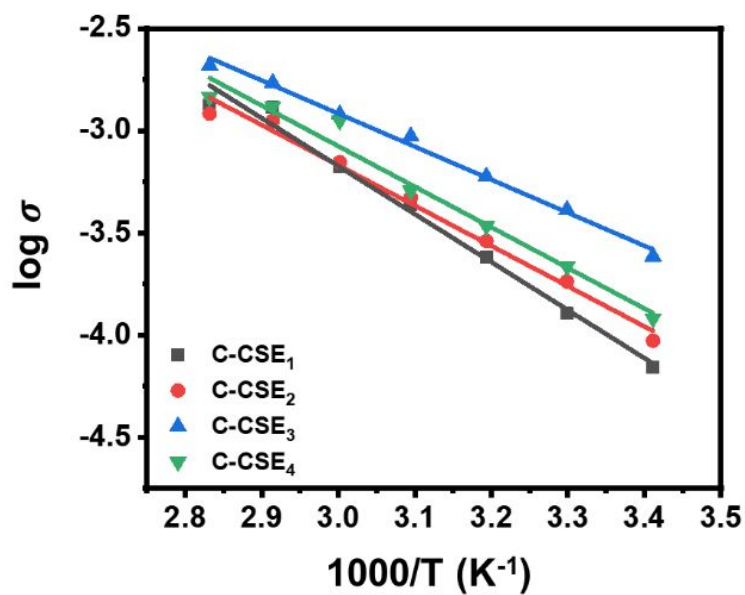
Figure S7. Arrhenius plots of C-CSE$_1$, C-CSE$_2$, C-CSE$_3$ and C-CSE$_4$.
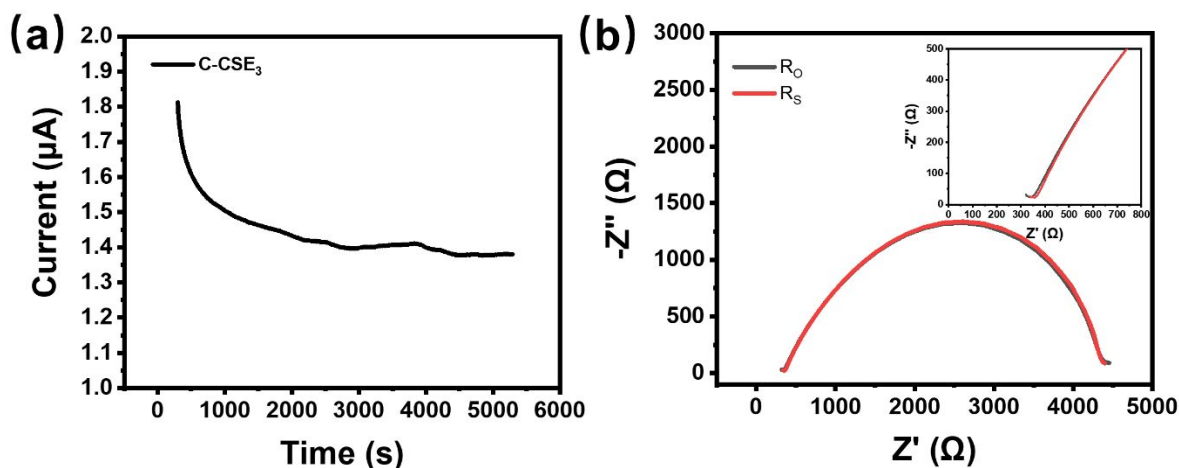
Figure S8. (a) Variation of current with time during polarization at an applied voltage of 10 mV at 25 ℃. (b) EIS of lithium|C-CSE$_3$|lithium symmetric cell before and after polarization.
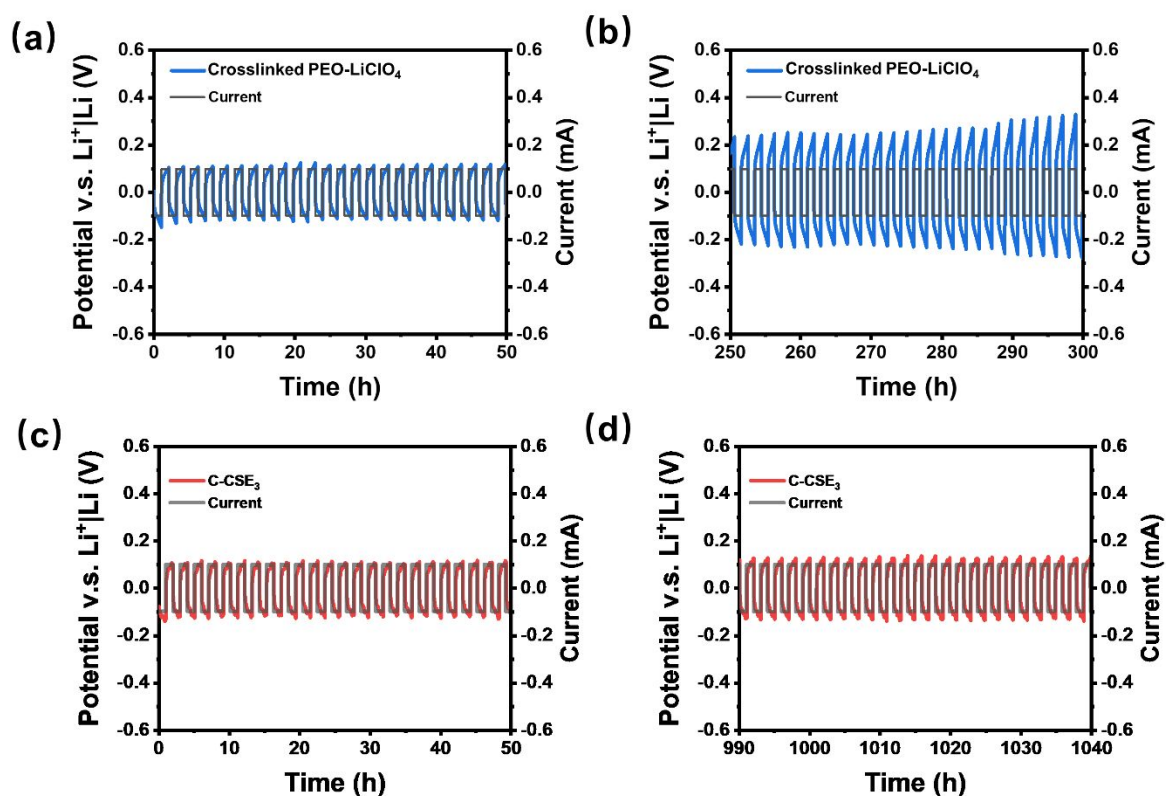
Figure S9. (a) The beginning cycling (0 ~ 50) of lithium|Crosslinked PEO-LiClO$_4$|lithium symmetric battery. (b) The final cycling (250 ~ 300) of lithium|Crosslinked PEO-LiClO$_4$|lithium symmetric battery. (c) The beginning cycling (0 ~ 50) of lithium|C-CSE$_3$|lithium symmetric battery. (d) The final cycling (990 ~ 1040) of lithium| C-CSE$_3$|lithium symmetric battery.

Table 1. Ionic conductivity and Ea of different samples.

Samples	Ionic conductivity (S cm^{-1})	Ea (eV)
PEO-LiClO$_4$	2.99×10^{-6}	0.77
CSE	2.22×10^{-5}	0.53
C-CSE$_1$	1.28×10^{-4}	0.46
C-CSE$_2$	2.06×10^{-4}	0.39
C-CSE$_3$	4.26×10^{-4}	0.25
C-CSE$_4$	2.45×10^{-4}	0.40

Table 2. The performance comparison of the C-CSE$_3$ with other type MOF-based electrolyte.

Electrolyte type	Ionic conductivity (S cm^{-1})	Electrochemical window (V)	Li-ions transference number	Lithium compatibility	Ea (eV)	Reference
LLZO · UIO-67(Zr) (LLZO=Li$_{6.25}$Al$_{0.25}$La$_3$Zr$_2$O$_{12}$)	1.00×10^{-4}	5.2	0.18	38 days	/	[2]
2D, cationic framework	5.74×10^{-5} (300K)	3.7	0.61±0.02	/	0.34	[6]
Mg$_2$(dobdc)·0.35LiOi Pr·0.25LiBF$_4$· EC · DEC (EC=ethylene carbonate; DEC=diethyl carbonate)	3.1×10^{-4} (300K)	/	/	/	0.15	[7]
MOF-525(Cu) · Ionic liquid	3.0×10^{-4} (RT)	4.1	0.36	8 days	/	[8]
MOF(Cu)-modified electrolyte (1M LiTFSI in DOL/DME)	7×10^{-5}	4.5	0.7	800 h	/	[9]
M-UiO-66-NH$_2$-PEGDA	4.31×10^{-5} (303K)	5.5	/	550 h	/	[10]
Crosslinking CSE (PEO-LiClO$_4$-ZIL; ZIL=ZIF-8·LiTFSI·IL)	4.26×10^{-4} (300K)	> 5.2	0.67±0.08 (300K)	> 1040 h (300K)	0.25	**This Work**

References

(1)　Fujie, K.; Yamada, T.; Ikeda, R.; Kitagawa, H., Introduction of an ionic liquid into the micropores of a metal-organic framework and its anomalous phase behavior. *Angew. Chem. Int. Ed.* **2014,** *53* (42), 11302-11305.

(2)　Wang, Z.; Wang, Z.; Yang, L.; Wang, H.; Song, Y.; Han, L.; Yang, K.; Hu, J.; Chen, H.; Pan, F., Boosting interfacial Li$^+$ transport with a MOF-based ionic conductor for solid-state batteries. *Nano Energy* **2018,** *49*, 580-587.

(3)　Bae, J.; Li, Y.; Zhang, J.; Zhou, X.; Zhao, F.; Shi, Y.; Goodenough, J. B.; Yu, G., A 3D Nanostructured Hydrogel-Framework-Derived High-Performance Composite Polymer Lithium-Ion Electrolyte. *Angew. Chem. Int. Ed.* **2018,** *57*, 2096-2100.

(4)　Kresse, G.; Furthmüller, J., Efficiency of Ab-Initio Total Energy Calculations for Metals and Semiconductors Using a Plane-Wave Basis Set. *Comp. Mater. Sci.* **1996,** *6*, 15-50.

(5)　Kresse, G.; Furthmüller, J., Efficient Iterative Schemes for Ab Initio Total-Energy Calculations Using a Plane-Wave Basis Set. *Phys. Rev. B* **1996,** *54*, 11169-11186.

(6)　Chen, H.; Tu, H.; Hu, C.; Liu, Y.; Dong, D.; Sun, Y.; Dai, Y.; Wang, S.; Qian, H.; Lin, Z.; Chen, L., Cationic Covalent Organic Framework Nanosheets for Fast Li-Ion Conduction. *J. Am. Chem. Soc.* **2018,** *140* (3), 896-899.

(7)　Wiers, B. M.; Foo, M. L.; Balsara, N. P.; Long, J. R., A solid lithium electrolyte via addition of lithium isopropoxide to a metal-organic framework with open metal sites. *J. Am. Chem. Soc.* **2011,** *133* (37), 14522-14525.

(8)　Wang, Z.; Tan, R.; Wang, H.; Yang, L.; Hu, J.; Chen, H.; Pan, F., A Metal-Organic-Framework-Based Electrolyte with Nanowetted Interfaces for High-Energy-Density Solid-State Lithium Battery. *Adv. Mater.* **2017,** *30*, 1704436.

(9)　Bai, S.; Sun, Y.; Yi, J.; He, Y.; Qiao, Y.; Zhou, H., High-Power Li-Metal Anode Enabled by Metal-Organic Framework Modified Electrolyte. *Joule* **2018,** *2* (10), 2117-2132.

(10) Wang, Z.; Wang, S.; Wang, A.; Liu, X.; Chen, J.; Zeng, Q.; Zhang, L.; Liu, W.; Zhang, L., Covalently linked metal–organic framework (MOF)-polymer all-solid-state electrolyte membranes for room temperature high performance lithium batteries. *J. Mater. Chem. A* **2018,** *6* (35), 17227-17234.